

Finite element tree crown hydrodynamics model (FETCH) using porous media flow within branching elements: A new representation of tree hydrodynamics

Gil Bohrer, Hashem Mourad, Tod A. Laursen, Darren Drewry, and Roni Avissar

Department of Civil and Environmental Engineering, Duke University, Durham, North Carolina, USA

Davide Poggi, Ram Oren, and Gabriel G. Katul

Nicolas School of the Environment and Earth Sciences, Duke University, Durham, North Carolina, USA

Received 12 April 2005; revised 29 June 2005; accepted 28 July 2005; published 2 November 2005.

[1] Estimating transpiration and water flow in trees remains a major challenge for quantifying water exchange between the biosphere and the atmosphere. We develop a finite element tree crown hydrodynamics (FETCH) model that uses porous media equations for water flow in an explicit three-dimensional branching fractal tree-crown system. It also incorporates a first-order canopy-air turbulence closure model to generate the external forcing of the system. We use FETCH to conduct sensitivity analysis of transpirational dynamics to changes in canopy structure via two scaling parameters for branch thickness and conductance. We compare our results with the equivalent parameters of the commonly used resistor and resistor-capacitor representations of tree hydraulics. We show that the apparent temporal and vertical variability in these parameters strongly depends on structure. We suggest that following empirical calibration and validation, FETCH could be used as a platform for calibrating the “scaling laws” between tree structure and hydrodynamics and for surface parameterization in meteorological and hydrological models.

Citation: Bohrer, G., H. Mourad, T. A. Laursen, D. Drewry, R. Avissar, D. Poggi, R. Oren, and G. G. Katul (2005), Finite element tree crown hydrodynamics model (FETCH) using porous media flow within branching elements: A new representation of tree hydrodynamics, *Water Resour. Res.*, 41, W11404, doi:10.1029/2005WR004181.

1. Introduction

[2] Over the past two decades, the role of photosynthetically active radiation (PAR) and vapor pressure deficit (VPD) in regulating stomatal conductance [e.g., *Leuning*, 1995; *Oren et al.*, 1999a] and photosynthesis [*Farquhar et al.*, 1980; *Collatz et al.*, 1991] has been made clearer, and progress has been made in scaling these processes to the canopy level. In particular, the nonlinear interaction between light and leaf photosynthesis necessitates a multilevel description of the canopy to scale leaf-level processes up to the canopy scale [*Baldocchi*, 1992; *Baldocchi and Meyers*, 1998; *Lai et al.*, 2000b, 2002; *Schäfer et al.*, 2003]. There is a growing recognition that plant hydraulics also play a central role in linking root water uptake to transpiration and carbon uptake [e.g., *Sperry et al.*, 1998; *Katul et al.*, 2003; *Brodribb and Holbrook*, 2004]. A mechanistic understanding of the effects of soil-plant hydraulics on transpiration must account for water movement within the tree system and the potential onset of xylem cavitation [*Sperry*, 2000; *Sperry et al.*, 2002].

[3] However, unlike canopy radiation models, in which plant area density can be treated as a random medium (with clumping), plant hydrodynamics must resolve the plant

architecture, allometry, and branching. Several factors frustrate modeling water movement within the tree system, as summarized below:

[4] The first factor is computational. Although it is possible to derive point equations for flow within one organ element, solving a transient nonlinear diffusion equation in high-resolution 3-D on an unstructured mesh needs a large computational resource.

[5] The second factor is data availability. Although few studies quantify the hydraulic properties of trees [*Maherali and DeLucia*, 2001; *Domec and Gartner*, 2003; *Brodribb and Holbrook*, 2004; *Chuang et al.*, 2005], measurements conducted with the intent to model water flow through all the plant organs are scarce.

[6] The third factor is relevance to ecohydrologic models. Little information exists as to whether differences in tree level structure lead to consistent biases that accumulate at scales relevant to the canopy [e.g., *Goldstein et al.*, 1998; *Ewers et al.*, 2001; *Köstner*, 2001; *Maherali and DeLucia*, 2001; *Domec and Gartner*, 2003; *Meinzer et al.*, 2003]. An essential question is whether these effects can be formalized into scaling laws, and whether the architecture of the crown is beneficial for diagnostic and prognostic hydrologic models. This is the subject of this study.

[7] Although this study does not offer new empirical data, it makes use of published empirical parameters to derive a novel numerical model, the finite element

Electric equivalence models – ODE

Porous media models – PDE

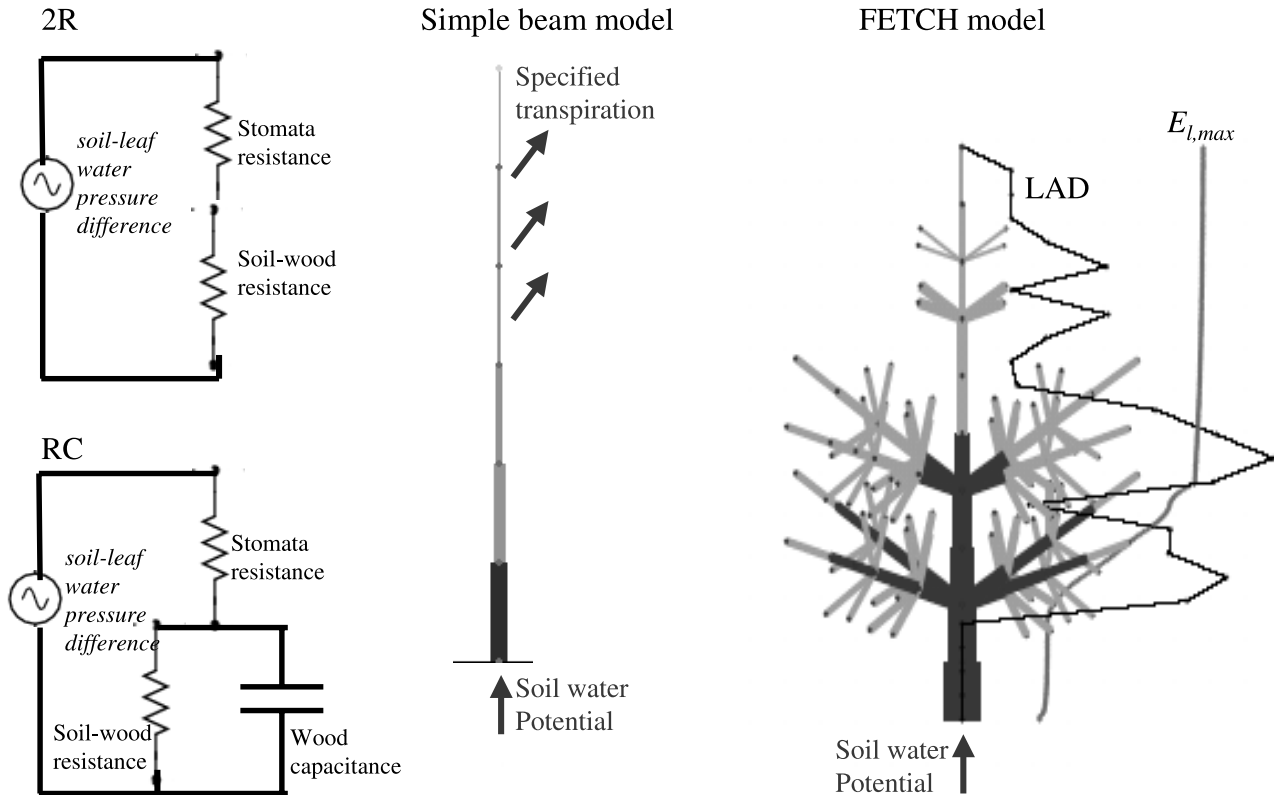


Figure 1. Canopy representation in atmospheric and hydrologic models. A two-resistor model (2R) neglects the capacitance and canopy structure, a resistor capacitor model (RC) that corrects for storage, a simplified porous media vertical beam model with tapering that does not account for branching and the distribution of LAD , and the proposed FETCH model that represents a full tree structure and fully linked to its microclimate in terms of light, CO_2 concentration, temperature, VPD , and wind statistics. Here we present a sample L-system tree; bold lines represent the branches. Shaded branches are leaves supporting “end branches” that transpire. Black profile marks LAD . Gray profile is noontime potential leaf transpiration ($E_{l,max}$).

tree crown hydrodynamics (FETCH) model. This model resolves plant hydrodynamics across a range of realistic tree structures. This model is coupled to tree microclimate through radiative transfer and simplified turbulent transport theories. Using this new framework, we explore the sensitivity of plant hydrodynamics to canopy structure via parametric variations of simple scaling laws. The goal of this study is to highlight the advantages of this new modeling approach relative to the commonly used models of plant contribution to land-surface energy balance. These advantages include better temporal description of water fluxes from a tree crown and detailed vertical distribution. We suggest that by adopting this hydrodynamic description of the plant system, it is possible to better predict nonlinear, hard-to-parameterize phenomena such as midday stomata closure and differential stomatal response along a branch and incorporate the effects of tree structure and physiology in the prediction of changes in transpiration fluxes following environmental changes such as fertilization.

[8] The common models of tree-water systems incorporated within meteorological land-surface models are based on equivalence to an electric circuit (Figure 1). The most simple of these water flow models are the single (1R) or multiple (2R) resistor models [Jones, 1992]. These lump all vegetation below the grid resolution to a single effective “big leaf,” or to a low number of subgrid patches. Some examples for “big leaf” resistor models include SiB2 [Sellers *et al.*, 1996a, 1996b] and LEAF2 [Walko *et al.*, 2000]. The resistor models take no account of water storage in the plant and therefore assume constant equilibrium between transpiration and the energy gradients between the soil and the atmosphere (see Figure 1). The resistance-capacitance (RC) models are another type of electric circuit equivalence model developed to account for water storage (or “charge capacitance”), which is presumably important in tall forested ecosystems [Jones, 1992; Schulte and Costa, 1996; Phillips *et al.*, 1997]. The resistance and capacitance are empirical properties often calibrated to match observa-

tions. It is possible to represent a crown structure using a RC model, but that would require branch level or crown/canopy-layer level empirical calibration [Jones, 1992].

[9] A more physically based approach is to combine the continuity equation with a physical transport law applied to an elemental organ, which leads to a nonlinear partial differential equation (PDE) resembling Richards' equation for soil water movement including sources and sinks. In essence, this approach assumes that water movement through a collection of interconnected tracheids in the hydroactive xylem (typical to conifers) resembles porous media flow [Siau, 1983; Fröh and Kurth, 1999; Kumagai, 2001; Chuang et al., 2005]. This view is perhaps indirectly supported by the wealth of hydraulic cavitation curves collected for various plant organs that are analogous to hydraulic losses in porous media (e.g., Sperry [2000] and review by Feild et al. [2002]). As discussed by Chuang et al. [2005], the mathematical properties (and boundary conditions) of the resulting porous-media PDEs may significantly diverge from RC models whose mathematical properties are first-order ordinary differential equations for the water flux.

[10] Treating sap flow in wood as porous media flow to apply Darcy's law was first suggested by Siau [1983]. Arbogast et al. [1993] developed a Richards-type equation as a way to numerically solve water movement in lateral roots as part of a soil water system. A branch system was suggested by Fröh and Kurth [1999], who generated a splitting-branch tree-grid system and solved it using finite differences. A similar but somewhat simplified approach was also developed by Kumagai [2001] and later adopted by Chuang et al. [2005], who revised it to include nonlinear terms for the conductance and capacitance. All of the above require specified transpiration from each branch as a model input. The stem systems in the latter two studies were limited to a single stem without branching (see Figure 1).

[11] An even more complete model of the tree transport system was suggested by Aumann and Ford [2002a, 2002b]. They observed that a tracheid-level model could lead to a better representation of the flow in nonsaturated stages, for example, when recovering from cavitations. The need, though, for many cell-level parameters and explicit cell-structure element construction makes it less attractive as a general simulation tool. Furthermore, none of the above models considers interaction between the tree and its microclimate.

[12] Here we adopt the formulation of Chuang et al. [2005] and adjust it to handle a nonvertical branching system, similar to that proposed by Fröh and Kurth [1999]. We also added a multiple-layer canopy microclimate model using leaf-level physiological, radiative transfer, and canopy drag properties as discussed by Lai et al. [2000a] with a first-order turbulent closure scheme [Poggi et al., 2004], and add a stomatal response that links pressure in the branches to stomatal resistance. The resulting FETCH model simulates the hydrodynamics of a branching pipe system, constructed in a manner to be consistent with the plant area density. The model also utilizes the "aorta" or "fully coupled" tree transport system formulation [McCulloh et al., 2003; Schulte and Brooks, 2003]. This approach assumes free flow along the radial axis of the branches.

[13] By using such a physically based plant-atmosphere-hydraulics model with explicit three-dimensional (3-D) representation of the tree structure, we can confront the question of how the variability in crown architecture (i.e., interspecific, age, or ecosystem dependent structure) would lead to different transpiration responses. We compare the results from such a detailed model with the equivalent resistance and capacitance parameters that would have been obtained by 2R and RC models (see Figure 1). This comparison is used to test the sensitivity of the tree system to structure and its consequent effects on 2R or RC parameterizations that do not and in most cases cannot include structural aspects of the tree.

2. Materials and Methods

2.1. Governing Equations

[14] Upon horizontal averaging a cross-sectional plane that includes a collection of tracheids, we can adopt a porous media analogy using a 1-D Richards equation for the water pressure along the hydraulic path length l :

$$C(\Phi) \frac{\partial \Phi}{\partial t} = \frac{\partial}{\partial l} \left[k(\Phi) \left(\frac{\partial \Psi}{\partial l} \right) \right] + S_{nk}. \quad (1)$$

In a vertical branch segment ($l = z$), the total water potential (Ψ) is related to the water pressure (Φ) by the equation $\Psi = \Phi + \rho g l$. The capacity $C(\Phi)$ and xylem conductivity $k(\Phi)$ are nonlinear functions of Φ . S_{nk} represents all water sinks and sources including water loss by transpiration. A key assumption in equation (1) is that water transport is driven primarily by pressure and gravitational potential differences and not dominated by other forcing such as solute potential differences. Units and descriptions for the symbols used in this and all other equations below appear in Table 1.

[15] The system we use to represent a tree is an assortment of 1-D branches, but the nonvertical branches add volume to the system and thus turn it to a 3-D rather than a 1-D system. For further computational efficiency, we obtain a strict 1-D representation of this 3-D structure by using a conversion term, $\cos(\alpha)$, for the hydrostatic pressure to correct for the angle between the branch element and zenith (α) in nonvertical branches (where the path length l is longer than its vertical component z). This yields the following PDE system:

$$\left\{ \begin{array}{l} C(\Phi) \frac{\partial \Phi}{\partial t} = \frac{\partial}{\partial z} \left[k(\Phi) \left(\frac{\partial \Phi}{\partial z} + \rho g \cos(\alpha) \right) \right] - E_V \\ \Phi|_{z=0} = \Psi_s \\ \frac{\partial \Phi}{\partial z} \Big|_{z=\text{end of branch}} = 0 \\ \Phi(z)|_{t=0} = \Psi_s - \rho g z \end{array} \right. \quad (2)$$

[16] This representation allows expressing the coordinates system only in the vertical direction (z , positive above the ground). We neglect all other sources or sinks of water other than transpiration (E_V). We assume Dirichlet boundary conditions at the bottom of the trunk (i.e., the "stem-root interface"). When soil is saturated, pressure at the top of the root system can be assumed constant and near saturation. Thus we treat the pressure at this boundary as surrogate for soil water pressure (Ψ_s). In the current simulations, $\{\Psi\}_s$

Table 1. Notation^a

Symbol	Description	Units	Value	Comments
d'	unit conversion coefficient	$\text{kg kPa}^{-1} \text{mol}^{-1}$		function of air density and temperature
A_{az}	hydraulically effective cross-sectional area of branch	m^2		
A_b	cross-sectional area of a branch	m^2		on a plane normal to the length
A_{can}	ground projection area of tree	m^2	5.56	density of 1800 trees/Ha, based on Ewers <i>et al.</i> [2001]
A_m	scaling coefficient for effective cross-sectional area	m^2	0.01	minimal stem area
A_{tot}	total cross-sectional area of a conductive system	m^2		
A_z	cross-sectional area of branch element	m^2		on a plane normal to the length
A_{zo}	cross-sectional area at tree base	m^2	0.68	
b'	minimal conductivity parameter of stomatal conductance model	$\text{mol m}^{-2} \text{s}$	0.01	Leuning [1995]
C	water capacity of xylem	kg m Pa^{-1}		
C_{tot}	tree-level capacity	kg m Pa^{-1}		
C_1	empirical curve fitting coefficient-cavitation pressure	Pa	4.8×10^{-6}	<i>Picea abies</i> [Mayr <i>et al.</i> , 2003]
c_2	empirical curve fitting coefficient for conductance		3.5	<i>Picea abies</i> [Chuang <i>et al.</i> , 2005]
c_3	empirical curve fitting coefficient for steepness of stomatal response		8	Cruziat <i>et al.</i> [2002]
c_4	empirical “thinning” coefficient		0.004	fitted between stem base and top diameters of 25 and 0.5 cm measured October 2001
C_a	CO ₂ concentration in air	ppm	380	
C_i	intracellular CO ₂ concentration	ppm		
D_0	scaling parameter of <i>VPD</i> in the stomatal conductance model	Pa	3000	Leuning [1995]
EB	“extra branch” coefficient in the scaling law that governs branch cross-sectional area		range 1–3 in steps of 0.2	in the “natural tree” $EB = 1.75$ [Oren <i>et al.</i> , 1986]
ED	“exponent order” coefficient in the scaling of conductivity and cross-sectional area		range 1.4–2.8 in steps of 0.2	in the “natural tree” $ED = 2.44$ [Cruziat <i>et al.</i> , 2002]
e_m	maximal quantum efficiency		0.08	Leuning [1995]
$E_{l,max}$	maximal leaf transpiration rate	$\text{kg m}^{-2} \text{s}$		
E_V	transpirational water sink	kg s^{-1}		
$E_{V,max}$	maximal potential transpiration	kg s^{-1}		no hydrologic limitations
E_{sf}	sap flux	kg s^{-1}		
g	gravitational acceleration	m s^{-2}	9.807	
k	xylem conductivity to water	$\text{m}^2 \text{s}$		
k_b	boundary-layer-air water conductance	$\mu\text{mol m}^{-2} \text{s}^{-1}$		function of wind speed
k_l	leaf to air water conductance	$\mu\text{mol m}^{-2} \text{s}^{-1}$		
k_{max}	maximal xylem conductance	$\text{m}^2 \text{s}$	1.36×10^{-8}	
l	hydraulic path length	m		
l_i	hydraulic path length from the ground to point i	m		
LAD	leaf area density	$\text{m}^2 \text{m}^{-1}$		
LAI	total leaf area index	$\text{m}_{leaf}^2 \text{m}_{ground}^{-2}$	6	Ewers <i>et al.</i> [2001]
lb	length along a side branch	m		
m	fitting parameter of stomatal conductance model		4	Leuning [1995]

Table 1. (continued)

Symbol	Description	Units	Value	Comments
m_c	Michaelis constant for CO ₂ fixation	ppm	300	Leuning [1995]
m_c	Michaelis constant for O ₂ inhibition	ppm	300,000	Leuning [1995]
NB	number of side branches at each split		4	
N_{el}	number of branch elements		114	
o_i	O ₂ mol fraction	ppm	210,000	Leuning [1995]
p	empirical curve fitting coefficient for water content		20	
PAR	photosynthetic active radiation	$\mu\text{mol m}^{-2} \text{s}^{-1}$	measured	Duke Forest, October 2001
R_l	leaf resistance in 2R model	Pa s kg^{-1}		
$R_{l,\text{min}}$	minimal leaf resistance	Pa s kg^{-1}		assuming no hydraulic limitations
R_p	total “per tree” resistance (leaf + wood) in RC model	Pa s kg^{-1}		
R_s	wood resistance in 2R model	Pa s kg^{-1}		stem + branches
S_{nk}	total water sink	kg s^{-1}		
S_{tot}	total tree storage	kg		
t	time	s		
$V_{c,\text{max}}$	maximal carboxylation capacity of Rubisco	$\mu\text{mol m}^{-2} \text{s}^{-1}$	59	Leuning [1995]
V_d	dark respiration	$\mu\text{mol m}^{-2} \text{s}^{-1}$	$0.015V_{c,\text{max}}$	Leuning [1995]
VPD	vapor pressure deficit in air	kPa	measured	Duke Forest, October 2001
z	vertical height	m		
Φ	water pressure	Pa		
Φ_a	water pressure air	Pa		equivalent liquid phase pressure
Φ_l	water pressure in leaves petiole, end of branches	Pa		
Φ_s	water pressure at base of stem	Pa	-783.77	= $\{\Psi\}_s$, “soil” pressure
Φ_{tot}	“tree level” pressure	Pa		volume averaged
Φ_0	empirical parameter for water pressure of dry xylem	Pa	5.74×10^8	
Φ_σ	empirical critical pressure where stomata are half close	Pa	200,000	Cruziat <i>et al.</i> [2002]
Γ^*	compensation point for CO ₂ in the absence of dark respiration	ppm	60	Leuning [1995]
$\{\Psi\}$	total water potential	Pa		
$\{\Psi\}_s$	water potential at base of stem	Pa	-783.77	represents soil at near saturation
α	zenith angle of branch element	deg		
B_1	Farquhar coefficient for transpiration	$\mu\text{mol m}^{-2} \text{s}^{-1}$		Farquhar <i>et al.</i> [1980]
B_2	Farquhar coefficient for respiration	ppm		Farquhar <i>et al.</i> [1980]
β_p	leaf absorptivity for PAR		0.8	Leuning [1995]
θ	water content	kg m^{-3}		
θ_{sat}	water content at saturation	kg m^{-3}	573.5	<i>Picea abies</i> [Chuang <i>et al.</i> , 2005]
ρ	water density	kg m^{-3}	999	
τ	capacitor time constant	s		

^aParameters and coefficients values are shown with a reference (if applicable) to the source that parameterized or observed these values.

was kept constant and near saturation. Theoretically, in drying soil it would be possible to fit a decreasing pressure curve to this boundary that would simulate the roots' diminishing ability to extract water from the soil. At the top boundaries (i.e., at the end of branches), we set Neumann no-flux conditions, meaning water only exits the leaf-supporting branch elements via the transpiration sink term. Initial conditions are hydrostatic pressure equilibrium throughout the tree system.

[17] The equations for the hydraulic properties of the xylem system (the capacity and conductivity) can be derived and calibrated from empirical observations of wood properties [Sperry *et al.*, 1988; Alder *et al.*, 1997]. Trees' conductive systems, whether conifers or broadleaf, may be approximated by an anisotropic porous medium if capacitance and conductance are a priori calibrated. It is not our intent to diagnose those equations; instead, we use empirically fitted Weibull-shaped equations (equations (3) and (4)) to describe these

hydraulic properties. These Weibull-shaped equations for xylem vulnerability were observed for many species including conifers and broadleaf [e.g., *Tyree and Sperry, 1989; Sperry et al., 1994; Alder et al., 1997*]. Following *Chuang et al. [2005]*, we define the capacitance and conductance as

$$k(\Phi) = A_{az} k_{\max} \exp \left[- \left(\frac{-\Phi}{c_1} \right)^{c_2} \right] \quad (3)$$

$$C(\Phi) = A_z \frac{\partial \theta}{\partial \Phi} = \frac{A_z p \theta_{\text{sat}}}{\Phi_0} \left(\frac{\Phi_0 - \Phi}{\Phi_0} \right)^{-(p+1)} \quad (4)$$

A_z and A_{az} are the physical and effective hydraulic cross-sectional areas of the branch (see equation (9) for definition), and c_1 , c_2 , k_{\max} , θ_{sat} , Φ_0 , and p are empirical coefficients for the hydraulic system (see Table 1 for definitions and values). The FETCH model, as any other land-surface model, requires parameterization in order to correctly describe different species and biomes. Our model parameters c_1 , c_2 , k_{\max} , θ_{sat} , Φ_0 , and p can be determined by fitting the model's hydraulic parameters (in equations (3) and (4)) using sap-flux and atmospheric flux measurements.

[18] Unlike previous work in porous media flow in plants that solved the system using the finite difference approach [*Früh and Kurth, 1999; Kumagai, 2001; Aumann and Ford, 2002a; Chuang et al., 2005*], the FETCH model uses the finite element method (FE). FE has a particular advantage with the “aorta” branching pipe system because of the simplicity with which it handles the branching of the tree system in the element assembly process without the need to explicitly represent the structure of the junction in the element level formulation. The FE approach results in linearized 1-D element level equation system with a sparse diagonally banded tangent matrix that can be readily solved as described in Appendix A.

2.2. Maximum and Actual Transpiration

[19] For the vertical variation of maximal potential transpiration ($E_{V,\max}$) we use a multiple-layer coupled radiative-transfer, plant physiological, and turbulent transport model. This is used to calculate the relevant maximal potential transpiration that determined the water sink forcing of the tree system assuming maximal stomatal conductance is regulated by photosynthesis and thus controlled only by CO_2 concentration (C_a), photosynthetically active radiation (PAR) and vapor pressure deficit (VPD) at a given level in the canopy. Our approach assumes that the plant would maximize its carbon gain as long as plant hydraulics pose no limitation [*Katul et al., 2003*].

[20] At the leaf scale, photosynthesis (P_n), maximal stomatal conductance (k_l), and intercellular CO_2 concentration (C_i) are given by the solution of the following algebraic system [*Leuning, 1995; Leuning et al., 1995; Leuning, 1997, 2002*]:

$$\left\{ \begin{array}{l} P_n = \frac{\beta_1 (C_i - \Gamma^*)}{C_i + \beta_2} - V_d \\ P_n = k_l C_a \left(1 - \frac{C_i}{C_a} \right) \\ k_l = \frac{m P_n}{C_a} \frac{1}{1 + VPD/D_o} + b' \\ \text{Light limited : } \beta_1 = \beta_p e_m PAR, \beta_2 = 2\Gamma^* \\ \text{Rubisco limited : } \beta_1 = V_{c,\max}, \beta_2 = m_c(1 + o_i/m_o) \end{array} \right. \quad (5)$$

(See Table 1 for definitions, sources, and values of the coefficients used in this equation set.) The maximum “leaf level” transpiration ($E_{l,\max}$) represents the transpiration water sink regardless of hydrological limitations, and is given by

$$E_{l,\max} \approx \beta' \left(\frac{k_s k_b}{k_s + k_b} \right) VPD, \quad (6)$$

where k_b is the boundary layer conductance (which varies with mean wind speed at a given level within the canopy), and β' is a constant for unit conversions (Table 1). Branch-level maximal transpiration ($E_{V,\max}$) depends on $E_{l,\max}$, total leaf area, and the leaf area density distribution (LAD).

[21] To compute PAR at each level within the canopy, an exponential extinction for a spherical leaf angle distribution with considerations for leaf clumping is employed [*Campbell and Norman, 1998*]. For this study, only beam radiation was considered, though it is possible to revise this formulation and include penumbral effects [*Stenberg, 1995*]. The model is forced by canopy-top values of PAR , air temperature, mean wind speed, and mean above canopy VPD . These values are updated every 15 min. To compute k_b , the wind speed at each level must be known. We used the mixing length and the turbulent closure model of *Poggi et al. [2004]* to compute the mean wind speed at each level within the canopy using the mean wind speed above the canopy. The calculations assume initially ambient scalar profiles of air temperature and relative humidity. It also assumes CO_2 concentration is equal to the canopy top value. As CO_2 uptake and water emissions occur, these profiles are then adjusted iteratively as described by *Lai et al. [2000a, 2000b]*. A sample vertical profile of $E_{l,\max}$ is shown in Figure 1 for noontime conditions. Note that while there is no foliage at the base of the tree, a finite $E_{l,\max}$ exists; however, this finite $E_{l,\max}$ does not contribute to the potential canopy transpiration when scaled with LAD .

[22] The actual transpiration water sink (E_V) depends on the stomatal response to “upstream xylem pressure” even when soil is saturated [*Oren et al., 1999b; Brodribb and Holbrook, 2004*]. This is represented in our model by the branch pressure at the transpiring element. Highly negative water pressure can lead to cavitation and loss of conductivity. Stomata have therefore evolved to reduce the water flux by increasing the leaf resistance to water loss (i.e., by closing the guard cells) when pressure is low [*Sperry et al., 1998; Oren et al., 1999a; Hubbard et al., 2001; Cruziat et al., 2002*]. The stomatal response is typically not instantaneous [*Sperry et al., 2003*]. Therefore, using the pressure at the previous time step (i.e., a 1-s lag) is justifiable. We expressed the evaporation water sink term as

$$E_V^{(n)} = E_{V,\max}^{(n)} \times \exp \left[- \left(\frac{-\Phi^{(n-1)}}{\Phi_\sigma} \right)^{c_3} \right], \quad (7)$$

where a superscript (n) marks the time step. Φ_σ and c_3 are hydraulic curve-fitting parameters (Table 1) and can be calibrated based on empirical “vulnerability curves” of leaf conductance or scaling laws between vulnerability of stem conductance and stomatal response [*Sperry, 1986; Oren et*

al., 1999a; Hubbard et al., 2001; Cruiziat et al., 2002; Addington et al., 2004].

2.3. Constructing the Model Trees: Scaling Structure

[23] Equations (1)–(7) have dealt with water flow and sinks at either the element or the crown level. Integrating these equations to the tree scale requires detailed representation of the tree architecture, which considers its branching geometry and architecture structural allometry. One of the popular models for branching-tree systems is based on the so-called L-system [Lindenmayer, 1968, 1971]. L-system has been successfully used to model a variety of plants at different stages of their growth, providing a convenient theoretical and programming framework for the architectural modeling of plants [Prusinkiewicz and Lindenmayer, 1990; Prusinkiewicz et al., 1997].

[24] Here we adopt the “turtle interpretation” [Szilard and Quinton, 1979] to construct the L-system. According to the “turtle interpretation,” a single set of instructions specifies a core series of “steps and turns,” each step adding a single element. This core series is repeated recursively to construct the full “tree.” The complexity level (set in this case to 2) controls the number of recursive iterations. The size and direction of each additional element (relative to the previous element) are controlled by two “structural” rules. The first rule controls the number and direction of additional branch elements at each branch junction (set in this study to 4 branches at 65° to the main axis). The second rule controls the branch cross-sectional area (see equation (8) for the formulation of this rule). An example application of these rules, representing the simplified “spruce” we used in our simulations, is shown in Figure 1.

[25] The cross-sectional area of branches emanating from any axis was represented by a linear function, decreasing with height:

$$\begin{cases} A_{zi} = A_{z0} - c_4 \times z_i \\ A_{bi} = EB \times \left(\frac{A_{z(i-1)} - A_{zi}}{NB} \right) - c_4 \times (l_i - z_i) \end{cases}, \quad (8)$$

where A_{zi} , A_{bi} are the physical cross-sectional area of a main and a side branch, respectively, at height level i , NB is the number of side branches at each split, and c_4 is an empirical “branch thinning” coefficient (Table 1). EB is referred to here as the “extra-branch” coefficient. EB represents the allometry of cross-sectional area distribution between the main stem and branches. It is expressed as the proportional coefficient between the cross-sectional areas, which are added to the tree by adding side branches, relative to the area lost by the narrowing of the main stem since the previous junction. It is a measure for the structural (carbon) cost of added conductive area.

[26] EB values can represent a wide range of hydraulic structures from the $EB = 1$ case, which is in essence, the “da Vinci scaling law” [Leonardo da Vinci, 1970], to more efficient structures specified by “Murray’s law” [Murray, 1926]. This law states that the optimal system should preserve the total volume, $A_{tot} \propto \Sigma r^3$, where r is the pipe radius, in the conductive pipes, and can be applied with some adjustments to vascular systems of plants, especially when accepting an aorta-like pipe system model [McCulloh

et al., 2003]. Murray’s law predicts that the total cross-sectional area of the plant hydraulic system would increase along the aboveground flow pathway in a tree as the radius of individual branches decrease. Values ranging significantly between Σr^2 and $\Sigma r^{4.5}$ (note that Σr^2 is equivalent to the da Vinci scaling law) in several tree species were observed by McCulloh et al. [2003]. An observed mean value for EB in *Picea abies* (L.) Karst (Norway spruce) is 1.75 [Oren et al., 1986].

[27] A plant stem or branch is not an empty pipe, and the cross-sectional area includes tissues that do not participate in axial water transport (e.g., bark, heartwood) and poorly conductive structural tissue (e.g., compression and tension wood). This implies that adding more cross-sectional area to existing branches can be more hydraulically efficient than adding a new thin branch. This leads to a functional relationship between the effective cross-sectional area of the branch and its conductivity. In an “empty-pipe,” the conductivity (k) is proportional to the cross-sectional area and scales with the diameter (d) to the second power, i.e., $k \propto d^{ED}$ where $ED = 2$. For a tree system not following an empty pipe model, ED , defined as the exponent order of conductivity, may exceed 2. ED smaller than 2 is also possible where heartwood exists in the thicker stem areas. Thus it is convenient to define an “effective hydraulic cross-sectional area” at level i (A_{azi}) as

$$A_{azi} = \left(\frac{A_{zi}}{A_m} \right)^{\frac{ED-2}{2}} \times A_{zi}. \quad (9)$$

Note that if $ED = 2$, then $A_{az} = A_z$. ED would be high in fast growing species because they grow by adding large, and thus hydraulically efficient, xylem elements and tracheids. ED would be low in drought-resistant plants that maximize cavitation resilience over hydraulic efficiency, and thus add narrow thick walled xylem elements and tracheids [Tyree, 2003]. Observations in several species found that ED values range between 2.41 and 2.79 [Cruiziat et al., 2002]. An observed ED for Norway spruce is 2.44 [Cruiziat et al., 2002].

[28] In summary, the combination of ED (a measure of the hydraulic efficiency gained by adding cross-sectional area) and EB (an architectural scaling law for the branch thickness) serves as a logical surrogate to evaluate the effects of crown architecture on its hydrodynamics in a virtual range of possible tree physiologies, representing different growth stages, environmental adaptations, and species.

2.4. Experimental Settings

[29] In this investigation we use a tree with four side branches, symmetrically splitting from the main branch or stem at each branch junction (Figure 1). End branches include the last members of each branch and all branch elements that are the sixth or farther from the bottom of the main stem (Figure 1). Only end branches carry leaves and lose water by transpiration. To roughly match a Norway spruce tree, we set the tree to be 12 m high (above the forest floor) with a branching angle of 65° and with 114 elements (branches and stem) of 1.2 m each. The base of the stem diameter is 0.25 m, tapering linearly up to 0.5 cm at the top. Leaf area index (LAI) is 6, and the total ground projection

area for the crown (A_{can}) is 5.56 m^2 , based on a Norway spruce stand [Ewers *et al.*, 2001], scaled to twice the height. We set the conductance coefficients c_1 and c_2 so that 50% xylem conductivity is lost when pressure reaches -4.2 MPa [Mayr *et al.*, 2003], and we set the stomatal curve fitting coefficients (Φ_σ and c_3) accordingly. We follow the rule that stomatal conductance would reduce 90% in response to 10% loss of xylem conductivity [Cruziat *et al.*, 2002]. Hence stomata of our model trees commence closure at branch pressure of -1.5 MPa and follow a Weibull reduction curve with reduced pressure until full closure at -2.5 MPa , as often reported for spruce [Cruziat *et al.*, 2002]. Calibration of the hydraulic coefficients (k_{\max} , θ_{sat} , Φ_0 , and p) was based on the work of Chuang *et al.* [2005] that empirically calibrated the dimensionless ratio ($k_{\max} \Phi_0 \theta_{\text{sat}}^{-1} p^{-1}$) based on sap-flux measurements at the same Norway spruce stand [Ewers *et al.*, 2001; Phillips *et al.*, 2004]. We kept this dimensionless ratio constant, and fixed θ_{sat} to its physically based value, and calibrated the other three coefficients. This calibration was done assuming that trees are naturally selected for “optimal transpiration,” and thus we fitted the coefficients to allow the natural tree to arbitrarily transpire about 90% of the maximal transpiration (3.66 mm/d [Phillips *et al.*, 2001, 2004]) and to fully recharge before 0500 LT (see Table 1 for coefficient values and units).

2.5. Comparing to Resistor and Resistor Capacitor Models

[30] To address the study objectives, we seek a connection between variations in ED and EB and the resulting time-dependent resistors and capacitors of the electric circuit analogy (Figure 1). The 2R model system can be represented by the following set of equations:

$$\begin{cases} E_{sf} = \frac{\Phi_l - \Phi_s}{R_s} = -E_V \\ -E_V = \frac{\Phi_a - \Phi_l}{R_l} \\ -E_{V,\max} = \frac{\Phi_a - \Phi_l}{R_{l,\min}} \end{cases}, \quad (10)$$

where E_{sf} is sap flux, Φ_l , Φ_s , and Φ_a are the liquid water pressure at the leaf petiole (i.e., at the ends of branches), the base of the stem (represents “soil” pressure), and in the air, respectively. R_s , R_l are “per tree” stem (i.e., all woody parts) and leaf resistance, $R_{l,\min}$ is the minimal “per tree” leaf resistance when stomata are fully open. Note that sap flux is equal to transpiration because the 2R model assumes no storage. By substituting the system in equation (10) into (7), we can obtain a solution for the equivalent leaf pressure:

$$\Phi_l = -\Phi_a \left[-\ln \left(\frac{E_V}{E_{V,\max}} \right) \right]^{\frac{1}{\beta}}. \quad (11)$$

The equivalent values of the two resistors are calculated as

$$\begin{cases} R_s = (\Phi_l - \Phi_s)/E_V \\ R_l = (\Phi_a - \Phi_l)/E_V \end{cases}. \quad (12)$$

[31] Another version of electric equivalence model is the resistor-capacitor analogy (RC) (see Figure 1), defined with

a time constant ($\tau = R_p C$) that determines the time it takes to empty 63% of the capacitor [Jones, 1992]. Here R_p is the total aboveground resistance of the tree. To compute the equivalent capacitance from our model, we first determine the storage of the whole tree (S_{tot}):

$$S_{tot} = \sum_{i=1}^{N_{el}} \int_{z_{ibase}}^{z_{itop}} \theta_{zi} \times A_{zi} dz, \quad (13)$$

where N_{el} is the total number of branch elements, z_{ibase} and z_{itop} are the height at the base and top of each element, and θ_{zi} is the local water content. Tree level capacitance (C_{tot}) and sap flux E_{sf} through the base of the stem at each time step can be calculated through the water mass balance:

$$C_{tot} = LAI \times A_{can} \times dS_{tot}/d\Phi_{tot} \quad (14)$$

$$E_{sf}|_{z=0} = E_V + dS_{tot}/dt, \quad (15)$$

where Φ_{tot} is a tree level pressure calculated by volume averaging Φ . LAI and A_{can} are used to convert the capacitance to consistent units with the “per-tree” resistance terms [Jones, 1992].

[32] Hence the effects of canopy architecture and allometry (i.e., EB and ED) on the electric-circuit-analogy models (Figure 1) can be directly assessed. As a first step, we focus on fully hydrated soil conditions (i.e., water pressure at base of stem held constant in time and close to saturation) to explore the effects of aboveground plant hydraulics on transpiration and storage.

3. Results and Discussion

[33] To address the study objectives, we simulated a total of 88 trees, with all combinations of ED and EB for a wide range of values between 1.0 and 3.0 (see Table 1). For reference, we define a “natural tree” with the scaling-parameter values $EB = 1.75$ and $ED = 2.44$, which were observed for Norway spruce. We will first show the temporal response of the “natural tree” to the canopy top meteorological forcing and relate the diurnal dynamics of the departure between actual transpiration and $E_{V,\max}$ to the pressure distribution and storage within various areas of the crown. Finally, we discuss the effects of crown architecture, through EB and ED , on the equivalent parameters of the 2R and RC circuit models (Figure 1).

3.1. Daily Dynamics of Evaporation and Sap Flux

[34] We simulated a period of 40 hours from 0500 LT of 1 August to 2100 LT the next day. The environmental conditions we use were smoothed long-term averages for that day over the Duke forest. The “natural tree” case was calibrated so that total daily transpiration would reach about 90% of the maximum transpiration that was reported by Chuang *et al.* [2005] and that storage would be restored to 99% of the initial conditions at 0400 LT of the second day (Figure 2). Our “natural tree” system displayed a daily transpiration and sap-flux cycle with a maximal transpiration peak at about 1130 LT and a sap flux peak lagging approximately 2.5 hours (Figure 2).

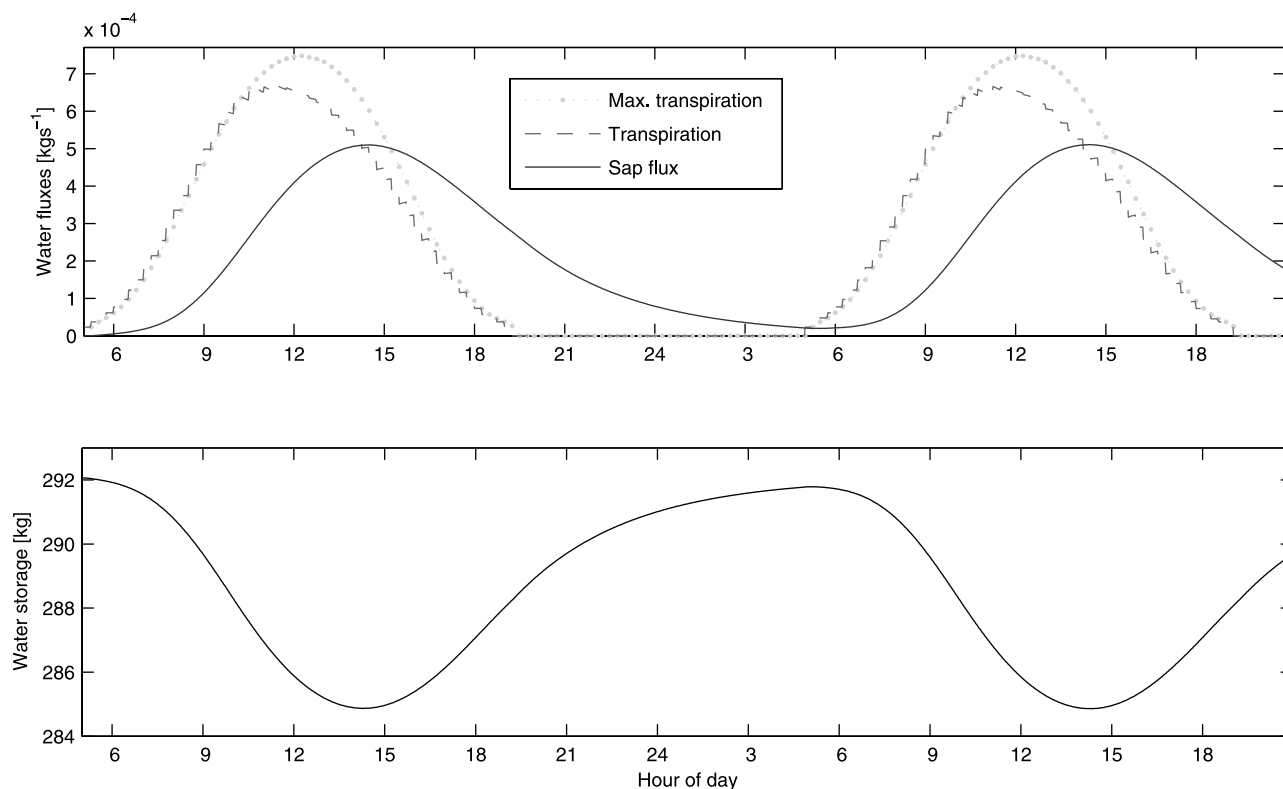


Figure 2. Tree-level water fluxes and storage. Dynamics of 40 hours in the simulated “natural tree” case. Top panel shows fluxes: maximal canopy potential transpiration (dotted curve), actual transpiration (dashed curve), and stem-base sap flux (solid curve). Bottom panel shows water storage.

[35] Actual measurements of sap flux differ widely between trees in the daily total amount of water transported. There are large differences between species, between sites, and between days within same trees, depending on the trees structure, soil moisture, and environmental conditions [e.g., Oren *et al.*, 1996; Phillips *et al.*, 1996; Oren *et al.*, 1998; Oren *et al.*, 1999a; Phillips *et al.*, 1999; Pataki *et al.*, 2000]. Typical transpiration and sap flux time series are much noisier than the smooth curves our model predicted. This is probably because our light function did not include shading effects by clouds, other trees, and branches and because our tree’s structure was simple and symmetric.

[36] Although we do not have the structural, environmental, and water flux data needed to fully calibrate and validate the model’s performance in comparison to a real tree in a particular day, qualitative comparisons can still be discussed. For example, early onset of the transpiration peak in Norway spruce in saturated soil was observed by Zweifel *et al.* [2001]. The length and strength of the lag between transpiration and sap flux are in agreement with values measured in Norway spruce trees by Herzog *et al.* [1998], and within the range of sap-flux-derived observations in other species, although in many examples it tends to be shorter than the one our model simulated [e.g., Goldstein *et al.*, 1998; Schäfer *et al.*, 2002; Meinzer *et al.*, 2003].

[37] Trees lost water from storage during the day and recovered to full storage at night (for the “natural tree,” see Figure 2). Figure 3 describes the time series of water pressure in different branches. The middle column shows results for structural parameters close to the “natural

tree” settings. When pressure drops below -1.5 MPa, stomata start closing. The model predicted earlier onset of midday closure of stomata on higher branches. These dynamics of midday stomatal closure are well documented, even in saturated soils (e.g., in spruce [Herzog *et al.*, 1998; Oren *et al.*, 2001; Zweifel *et al.*, 2002; Brodribb and Holbrook, 2004]), though they are not necessarily observed in all occasions. Our model also predicted the afternoon reopening of some of the stomata in the intermediate and high branches (Figure 3), consistent with Zweifel *et al.* [2002] who observed stomata reopening in upper branches.

3.2. Effect of Tree Structure

[38] For an analysis of the effects of *EB* and *ED*, we use only 13 hours of each simulation (i.e., 0600–1900 LT of 2 August). This is done to avoid artificial effects from the initial conditions. We focus primarily on the water pressure dynamics at various levels within the canopy because of their controls on leaf stomata.

[39] It is clear from Figures 3 and 4 that *EB* and *ED* affect the plant hydrodynamics in a nonlinear manner despite the hydrated soil conditions, the identical meteorological conditions above the canopy, and the identical leaf area and leaf-level physiological properties across the simulations. In all trees, pressure in the higher branches dropped faster than in the lower branches or those closer to the tree’s core (Figure 3). There are large differences, though, between trees with different structure (i.e., different values of *ED* and *EB*). In trees with thinner branches (lower *EB*) the branch

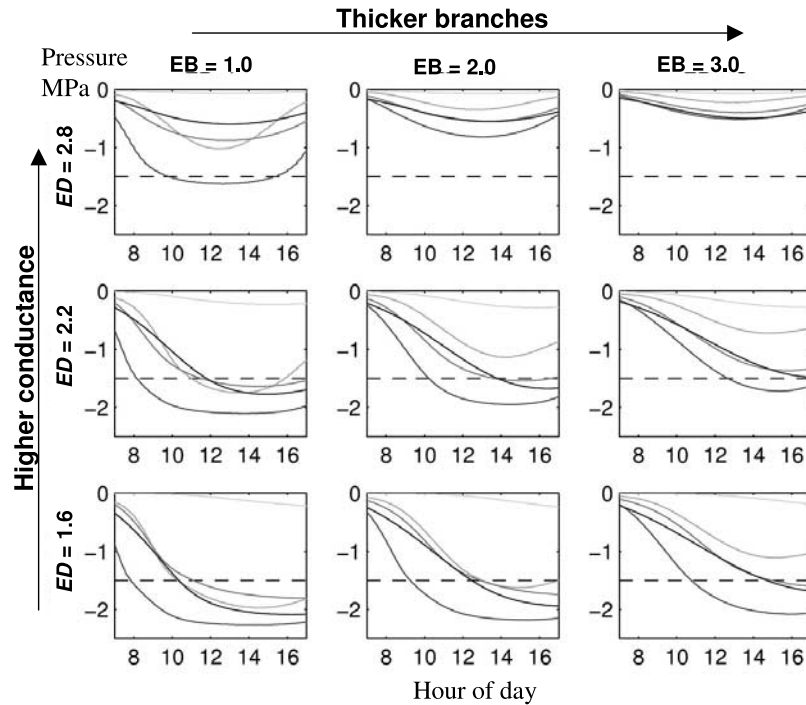


Figure 3. Pressure throughout the second day in different areas of the tree (y-axes, MPa). Different panels show different crown architectures with $ED = 1.6, 2.2, 2.8$ (bottom to top) and $EB = 1.0, 2.0, 3.0$ (left to right). The curves in each panel show the average pressure in a group of branch elements from a certain area of the crown, going from light (highest) to dark (lowest), the curves represent the pressure at the following areas: bottom part of the stem (ground to first split) ($z \in [1.2-2.4 \text{ m}]$), the lower end branches ($z \in [2.5-5.0 \text{ m}]$), the stem and branch bases in the middle part of the crown ($z \in [2.4-7.0 \text{ m}]$), midcrown end branches ($z \in [5.2-7.5 \text{ m}]$), and crown top ($z \in [8.5-12.0 \text{ m}]$). Note that stomata close between -1.5 (horizontal dashed line) and -2.5 MPa.

pressure drops faster and reaches the limiting pressure of -1.5 MPa earlier in the day, compared with branches at the same height in trees with thicker branches (Figure 3). These strongly negative pressures are the reason for the midday stomatal closure despite saturated soils. Trees with high conductive efficiency (i.e., high ED) are able to maintain higher levels of equilibrium water flow and therefore maintain less negative noontime branch pressures relative to branches of the same height in trees with lower ED . They also recover faster in the afternoon from the noontime pressure lows and are more likely to reopen stomata in higher branches (Figure 3).

[40] The structurally imposed differences in branch pressure and storage lead to different stomatal dynamics and thus change the daily transpiration and sap-flux dynamics (Figure 4). Trees with high EB draw more water from storage and their transpiration rate does not drop below the potential maximal transpiration for a long period throughout the day when compared with trees with low EB (see, in particular, Figure 4, middle column, where $ED = 2.8$). This effect was observed in a range of tropical tree species [Goldstein *et al.*, 1998]. Thus the simulation results demonstrate that total daily amounts of transpiration and change of storage are highly affected by tree structure: Although sap flux at the stem base is hardly affected by differences in EB , the transpiration peak can increase with EB due to water supplied from storage. Conversely, ED controls the maximal rate of sapflux: Low ED leads to lower

sap flux and longer lag time between maximal transpiration and maximal sap flux (Figure 4).

3.3. Equivalence to Electric Circuit Models

[41] On the basis of the simulations, crown architecture (simulated in this case through ED and EB) can inject different spatial and temporal responses in the equivalent parameters of 2R and RC circuit models. These models are currently the common parameterization approaches for determining the daily hydrodynamics of canopies. The notion of independent and constant values for capacitance and resistance (within a given set of external conditions such as soil moisture, VPD , temperature, and light intensity) is inherent in the electric equivalence models but cannot represent the tree hydraulic system. For example, the “capacitor discharge” of a branch not only reduces the available water storage but also increases the resistance of the drier branch and inhibits further discharge or recharge of the branch.

[42] In the 2R model, the main control on diurnal transpiration is the leaf resistance, while stem resistance, which accounts for the resistance of all woody parts of the tree, is either ignored, assumed to be constant, or assumed proportional to leaf resistance. Furthermore, leaf resistance is assumed to vary only as a function of external variables (e.g., VPD , soil moisture, temperature). With such parameterization, this approach cannot predict diurnal time lags between changes in water demand and dynamic pressure in

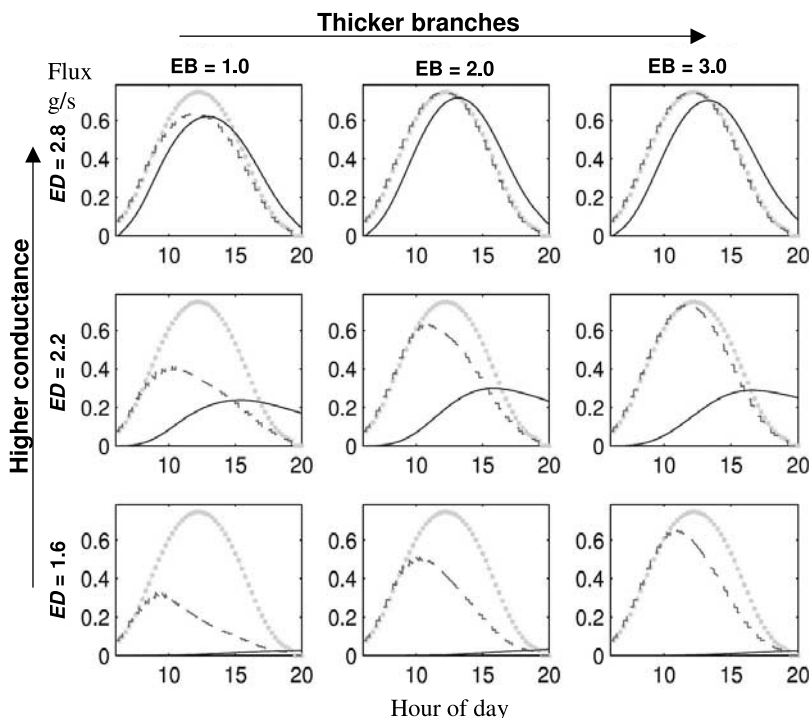


Figure 4. Water fluxes throughout the second day. Y-axes show the total maximal potential transpiration (dotted curve), total transpiration from the tree (dashed curve), and stem base sap flux (solid curve) in g s^{-1} . Panels showing different tree architecture, with $ED = 1.6, 2.2, 2.8$ (bottom to top), $EB = 1.0, 2.0, 3.0$ (left to right).

the stem [Phillips *et al.*, 2004]. The numerical results reported here suggest that none of these three representations are reasonable. Stem resistance was smaller than leaf resistance but still important ($R_s/R_l = 2\text{--}40\%$, Figure 5). Both stem and leaf resistances were highly affected by ED . With low ED , the leaf resistance increased rapidly throughout the day with a late afternoon peak (gray curves, Figure 5, top right panel). With high ED , leaf resistance was lower and less variable (black curves, Figure 5, top right). Stem resistance was relatively constant throughout the day with high ED (black curves, Figure 5, top left). With low ED , though, stem resistance was higher and had a rapid increase in the afternoon (gray curves, Figure 5, top left). The response of increased resistance at the afternoon for both leaf and stem was more pronounced for a tree with lower EB (solid curves, Figure 5, top panels). The relative size of stem resistance was larger with low ED (gray curves, Figure 5, lower left).

[43] In reality, leaf resistance is nonlinearly dependent on stem resistance. Plant stomata have evolved to regulate the stem pressure in order to prevent cavitation and respond to low stem pressure by closing the guard cells and increasing their resistance [Sperry *et al.*, 1998; Hubbard *et al.*, 2001; Oren *et al.*, 2001; Cruziat *et al.*, 2002; Sperry *et al.*, 2003]. This dependence might lead to different dynamic responses of leaf resistance in trees of different structures and in different environmental and climatic conditions that would be hard to calibrate empirically when using the common electric equivalence resistor models (other than a “per case” calibration).

[44] RC models are more flexible in their ability to represent different dynamic cycles and responses to envi-

ronmental forcing. Owing to the addition of an empirical time constant, they can represent the time lag between transpiration and sap-flux response. Typically, the resistor and capacitor coefficients are assumed constant in a given set of environmental conditions. By the definition of the capacitance in a porous media system, it is clear that C is a nonlinear function of the pressure, but the “working assumption” is that the diurnal variability in C is small and it can be averaged to a single capacitor constant [Jones, 1992; Phillips *et al.*, 1997]. Our simulations show that this is a good approximation when the branches are very thin ($EB = 1$, solid curves, Figure 5, bottom right) but not when branches are thick ($EB = 3$, dotted curves, Figure 5, bottom right). Branch structure (through EB) affects the capacitance more than the conductive efficiency (ED). Trees with high EB have up to a manyfold higher capacitance and tend to increase the capacitance more rapidly throughout the day (Figure 5, bottom right) when compared with their low EB counterpart. High ED tends to increase the capacitance but only in the thicker branches (Figure 5, bottom right). The range of C values estimated here is similar to the reported range for Norway spruce ($\sim 0.2 \times 10^{-7}$ [Phillips *et al.*, 2004]).

[45] Another advantage of RC models over 2R models is that they can be extended to represent a vertical canopy structure by including many independently calibrated capacitors. However, obtaining a realistically detailed description of a tree crown or a canopy system from such a multi-RC model requires specific empirical parameterization at the branch level or canopy-layer level that is very laborious and can rarely be practical. In addition, such parameterization can only be site specific and is not consistent among species, growth stages, and even seasons,

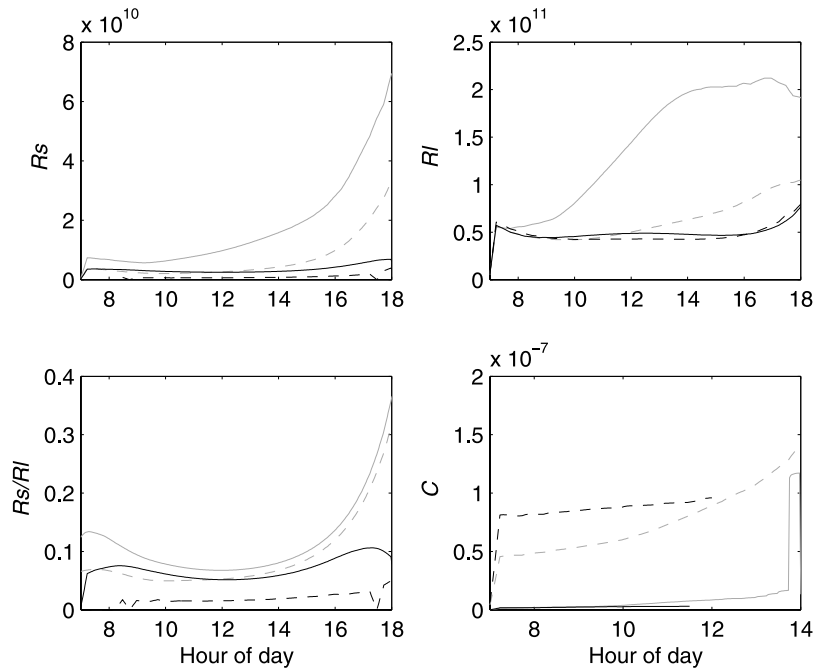


Figure 5. The temporal variation of the 2R and RC equivalent tree-level parameters. Panels show stem resistance (R_s , top left); leaf resistance (R_l , top right); the ratio between R_s and R_l (bottom left); and capacitance (C , bottom right). C is only calculated until 1400 LT (or shorter), it is ill defined when $d\Phi$ and dS are both near 0, and therefore we could not calculate an equivalent C around (and after) the time that sap flux exceeds total transpiration. Each panel is showing four trees with extreme architectures (in terms of ED and EB). Trees with $EB = 1$ are marked by a solid curve, $EB = 3$ by a dashed curve. Trees with $ED = 1.6$ are gray, $ED = 2.8$ are black.

because trees change their structure and their transpiration dynamics [e.g., *Tyree and Ewers, 1991; Borchert, 1994; Ryan et al., 2000; Köstner, 2001*]. Our simulations show that structural differences lead to marked differences in electric-equivalent parameters (Figures 5 and 6). Differences in conductance due to crown structure were observed in spruce trees [*Herzog et al., 1998; Rayment et al., 2000*].

[46] Typically, RC models do not operate at a branch level and thus lump all branches into a single- or multiple-layer representation. This approach is consistent with the atmospheric model representation of a horizontally layered grid but ignores the tree vertical structure. The result is a tree level time constant (τ). We find from our model calculations that τ is highly variable between trees with different crown structure (Figure 6). Here τ increases with higher EB but is also negatively affected by ED because τ is a product of resistance and capacitance and thus affected by both the conductive efficiency, which mostly modifies R_p , and the branch thickness, which mostly controls C . Trees with low conductance (high R_p) and thick branches (high C) have the longest τ . In the “natural tree,” $\tau = 15.33$ min, but depending on ED and EB , τ can vary from a few seconds to about 60 min. *Phillips et al. [2004]* showed that the RC model could be developed in a way that allows empirical calibration but requires introducing two different τ terms: a tree-level τ and a branch-level τ . They reported values of 5.4–6.4 min for the branch level and 48 min for the tree level in a Norway spruce. Our calculations of the time constant are mostly affected by the fluxes at the end branches, but also include the tree level C and therefore

represent an intermediate term between the tree and the branch level. This problem of ill-defined time constant (i.e., which part of the tree is considered in the discharge calculations) may explain why the reported τ varies appreciably among studies. For example, *Rayment et al. [2000]* reported a branch τ that ranges between 0.5 and 2 hours depending on the height. Also, *Chuang et al. [2005]* demonstrated that stem tapering can lead to significant changes in τ and reported an estimate of 1.25 hours from their model calculations, but their τ represented the time constant for nighttime recharge and not an RC equivalent daytime discharge. When these findings are all taken together, τ is likely to vary significantly with organ size, height, and structure, and throughout the day; hence the constant capacitance is an unrealistic representation of storage dynamics in the tree.

3.4. Scaling the Structure Effects in Time

[47] By integrating the transpiration rate over time, we can compare the total amounts of water transpired throughout the day by trees with different crown structure. In cases where the trees are fully replenished after a 24-hour cycle, this is also the amount of water that the tree transferred from the soil to the atmosphere. Trees with low ED or intermediate ED and low EB transpire much less than the maximal potential transpiration (as low as 20%), while trees with high ED reach 95% or more of the maximal potential transpiration (Figure 7). This response is due to pressure limitation that forces stomata to close in trees with suboptimal structure. At about 95% of potential, this response

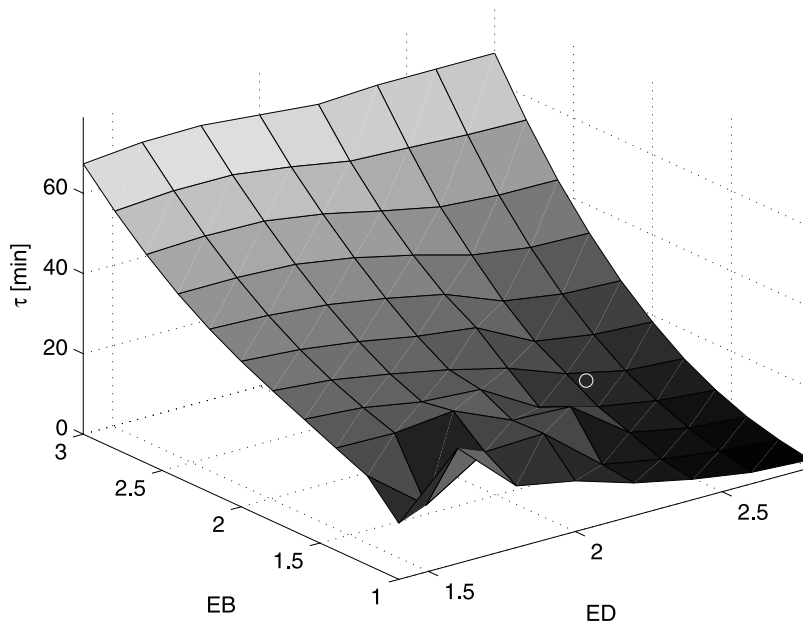


Figure 6. The mean RC equivalent time constant, $\tau = R_p C_{tot}$, as a function of ED and EB . Circle marks the “natural tree.”

saturates and very little additional transpirational gain is achieved for an additional increase of ED or EB . Such an increase must have a cost in terms of carbon allocation (bigger branches) or tradeoff with other functions of the branch (e.g., structural strength may be compromised to gain higher conductance for a given branch diameter), hinting at some optimization of conductive costs versus reduced transpiration and thus carbon gain. Combined with our findings about conductance, our model suggests that trees might adopt different structural strategies for different hydrological adaptations. Drought-resistant trees should

have high storage and low conductance [Tyree, 2003], and thus hydraulic structural properties typical to the upper left corner of our virtual structural plane (Figures 6 and 7) would be selectively preferred in a drought-resistant tree. Trees that optimize growth (and with it, transpiration rate) would be most efficient along the 95% contour of relative transpiration rate (Figure 7).

[48] We demonstrated that tree structure (through ED and EB) significantly impacts transpiration. This impact is apparent in the temporal and spatial (and in particular vertical) pattern of water fluxes from the canopy to the

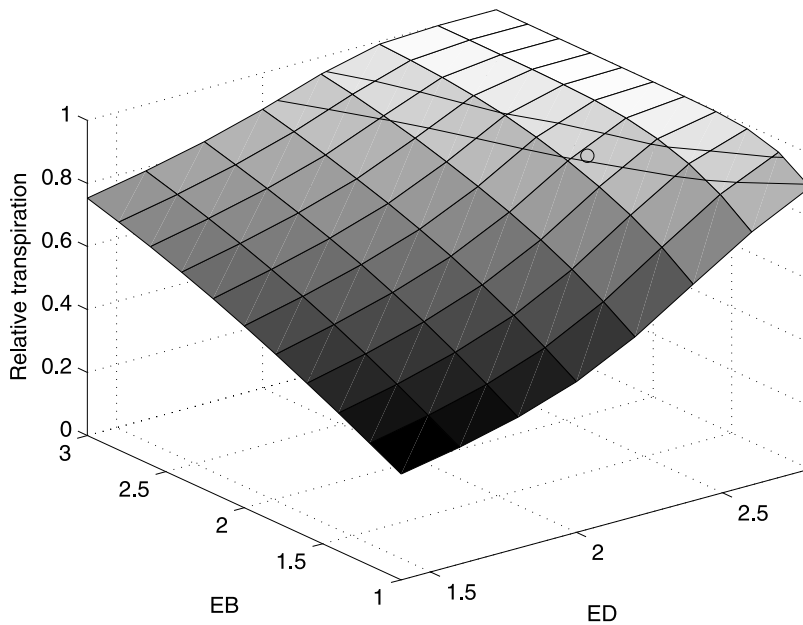


Figure 7. Relative transpiration, as the ratio between actual and maximal potential daily transpiration, represents the hydrologic efficiency of the tree in supplying water for transpiration. Lines mark 90% and 95% contours for hydrologic efficiency. Circle marks the “natural tree.”

air. We also showed that this impact accumulates to generate large differences in the total diurnal water flux from the soil to tree to atmosphere.

[49] That tree structure affects its hydraulic function and total daily transpiration is not new [Tyree and Ewers, 1991]. Differences in daily transpiration dynamics and totals were shown to be the result of structural differences due to fertilization [Ewers *et al.*, 2001], soil physical properties [Hacke *et al.*, 2000], seasonal phenology [Borchert, 1994], and different biomass allocation due to climate in different habitats [Maherali and DeLucia, 2001]. Tree age and height were shown to cause consistent differences in total transpirational flux [Ryan *et al.*, 2000; Schäfer *et al.*, 2000; Köstner, 2001; Addington *et al.*, 2004]. In particular, taller (older) trees were found to have lower daily transpiration rates per leaf area. As can be predicted from the model results, this is probably an effect of higher hydraulic stress in higher branches. Furthermore, on the basis of simulations, trees with higher stem capacitances are able to sustain higher transpiration throughout the day and in particular during noontime [Goldstein *et al.*, 1998; Meinzer *et al.*, 2003]. The consistency between the model results and observations suggests that this modeling approach offers a direct method to predict the structural effects on crown hydrodynamics via parameterization of scaling laws of crown structure and wood conductance. With further work, these effects could be scaled to represent the canopy on temporal and spatial scales that are relevant for regional meteorological and hydrological modeling.

4. Practical Considerations and Future Applications

[50] We proposed an organ-level hydrodynamic model with properties that can be independently derived. Given that the model uses conservation of mass and porous-media transport equations, it can be readily generalized to any woody species. Furthermore, unlike a laminar-flow pipe system, this approach preserves the nonlinear nature of the capacitance-conductance relationship through the structural allometry and hydraulic properties of the wood.

[51] FETCH is built as a modular combination of three independent modules: the porous media FEM solver, the fractal tree generator, and the turbulence-closure forcing module. The tree generator could be readily used to generate various structures that approximate observed crown scaling laws in order to study the ecological and evolutionary effects, and could also be replaced by actual tree measurements to link sap flux with transpiration in monitored sites. The meteorological forcing that now uses observations above the canopy could be replaced by a regional meteorological model such as RAMS [Pielke *et al.*, 1992]. Information about canopy morphology is becoming widely available, given the advancements in both canopy lidar measurements that can resolve the “coarse-tree branching” [see Lefsky *et al.*, 2002, Figure 9] and IKONOS imagery that can resolve crown width [Tanaka and Sugimura, 2001]. The fractal tree generator can readily incorporate such data to construct realistic trees.

[52] While several practical and theoretical difficulties remain, such as the applicability of Darcy’s law to water flow in xylems, and root dynamics and their relationship to soil moisture, the proposed approach is timely because it

provides a framework for confronting the challenges to modeling water flow in the plant-atmosphere system. We showed that the simplification achieved by the assembly of 1-D porous media pipes as a representation of the 3-D tree hydraulic system and the sparse banded symmetric structure of the tangent FE-solution matrix resulted in high computational efficiency. Hence the computational overhead of adding such a model (vis-à-vis the common models) in regional atmospheric, hydrologic, and ecological models is not high. Some examples of current models that link plant transpiration and atmospheric simulations and might benefit from an integrated FETCH approach, include LEAF [Walko *et al.*, 2000], VIC [Wood *et al.*, 1992; Liang *et al.*, 1994], SIB2 [Sellers *et al.*, 1996a, 1996b], and inference of water flux from the NOAA advanced very high resolution radiometer (AVHRR) instrument on board MODIS [Nishida *et al.*, 2003].

[53] In terms of relevance to ecohydrology, FETCH can account for the effects of forest structure on plant hydrodynamics, with subsequent effects on forest hydrology and carbon uptake [Schäfer *et al.*, 2000; Katul *et al.*, 2003]. Height was rarely considered in resistor-capacitor models that at best use calibrated static parameters with stand height. Following a rigorous phase of model validation, and given the potential availability and improvements in canopy lidar measurements, a FE porous media pipe system, such as FETCH, could replace current representations of plant hydrodynamics (e.g., 2R-big leaf, resistor-capacitor) and further contribute to the “greening” of climate models.

Appendix A: Development of the Finite Element Solution

[54] The strong form of the problem can be stated as follows:

Find $\Phi(z, t): \Omega \times \mathbb{R}^+ \rightarrow \mathbb{R}$ such that

$$C \frac{\partial \Phi}{\partial t} - k \frac{\partial}{\partial z} \left[\frac{\partial \Phi}{\partial z} + \rho g \cos(\alpha) \right] = -E_v \quad \text{in } \Omega, t > 0; \quad (\text{A1a})$$

$$\Phi = \Phi_s \quad \text{on } \Gamma_g, t \geq 0; \quad (\text{A1b})$$

$$\partial \Phi / \partial z + \rho g \cos(\alpha) = 0 \quad \text{on } \Gamma_h, t \geq 0; \quad (\text{A1c})$$

$$\Phi = \Psi_s - \rho g z \quad \text{in } \Omega, t = 0; \quad (\text{A1d})$$

[55] Multiplying (A1a) by a weighting function ω , and integrating by parts over the domain of interest Ω , we obtain

$$\begin{aligned} \int_{\Omega} \omega C \frac{\partial \Phi}{\partial t} d\Omega + \int_{\Omega} \frac{\partial \omega}{\partial z} k \left[\frac{\partial \Phi}{\partial z} + \rho g \cos(\alpha) \right] d\Omega \\ - \int_{\Gamma} \omega \left[\frac{\partial \Phi}{\partial z} + \rho g \cos(\alpha) \right] d\Gamma = - \int_{\Gamma} \omega E_v d\Omega. \end{aligned} \quad (\text{A2})$$

Defining the function spaces

$$\wp = \{ \Phi | \Phi \in H^1(\Omega), \Phi = \Phi_{soil} \text{ on } \Gamma_g \} \quad (\text{A3a})$$

$$\mathfrak{v} = \{ \omega | \omega \in H^1(\Omega), \omega = 0 \text{ on } \Gamma_g \}, \quad (\text{A3b})$$

where $H^1(\Omega)$ denotes the Hilbert space whose member functions, and their first-order derivatives, are square-integrable on Ω , we can state the weak form of the problem as follows:

Find $\Phi \in \wp$ such that, for all $\omega \in \nu$,

$$\int_{\Omega} \omega C \frac{\partial \Phi}{\partial t} d\Omega + \int_{\Omega} \frac{\partial \omega}{\partial z} k \left[\frac{\partial \Phi}{\partial z} + \rho g \cos(\alpha) \right] d\Omega = - \int_{\Omega} \omega E_v d\Omega. \quad (\text{A4})$$

It is noted that (A3a) ensures that the Dirichlet boundary condition (A1b) is satisfied. It is also noted that the boundary integral in (A2) does not appear in the weak form as the integrand vanishes on Γ_g , by virtue of (A3b), as well as on Γ_h , to satisfy the Neumann boundary condition (A1c).

[56] The domain is discretized into n_{el} element domains, denoted by Ω^e . Within an element with n_{en} nodal points, the trial solution and weighting function are approximated by their finite-dimensional counterparts, given by

$$\omega^h = \sum_{i=1}^{n_{en}} N_i c_i \quad (\text{A5a})$$

$$\Phi^h = \sum_{i=1}^{n_{en}} N_i d_i. \quad (\text{A5b})$$

Here $(\cdot)^h$ is used to denote a finite-dimensional function; N_i , d_i , and c_i are the shape function, the unknown nodal value of Φ^h , and the arbitrary nodal value of ω^h , respectively, belonging to node i . The Galerkin weak form can then be expressed as a summation of integrals over the individual elements:

$$\begin{aligned} \sum_{e=1}^{n_{el}} \int_{\Omega^e} \omega^h C \frac{\partial \Phi^h}{\partial z} d\Omega + \sum_{e=1}^{n_{el}} \int_{\Omega^e} \frac{\partial \omega^h}{\partial z} k \frac{\partial \Phi^h}{\partial z} d\Omega \\ + \sum_{e=1}^{n_{el}} \int_{\Omega^e} \frac{\partial \omega^h}{\partial z} k \rho g \cos(\alpha) d\Omega = - \sum_{e=1}^{n_{el}} \int_{\Omega^e} \omega^h E_v d\Omega. \end{aligned} \quad (\text{A6})$$

[57] Substituting (A5) into (A6) leads to a matrix equation of the form

$$\mathbf{M} \partial \mathbf{d} / \partial t + \mathbf{K} \mathbf{d} + \mathbf{F}^{\text{int}} = \mathbf{F}^{\text{ext}}, \quad (\text{A7})$$

where $\partial \mathbf{d} / \partial t$ and \mathbf{d} are the vectors of nodal unknowns of $\partial \Phi / \partial t$ and Φ , respectively. The ‘‘mass’’ matrix \mathbf{M} and the ‘‘stiffness’’ matrix \mathbf{K} are given by

$$\mathbf{M}_{ij} = \sum_{e=1}^{n_{el}} \int_{\Omega^e} N_i C N_j d\Omega \quad (\text{A8a})$$

$$\mathbf{K}_{ij} = \sum_{e=1}^{n_{el}} \int_{\Omega^e} \frac{\partial N_i}{\partial z} k \frac{\partial N_j}{\partial z} d\Omega, \quad (\text{A8b})$$

and the internal and external ‘‘force’’ vectors, \mathbf{F}^{int} and \mathbf{F}^{ext} , are given by

$$\mathbf{F}_i^{\text{int}} = \sum_{e=1}^{n_{el}} \int_{\Omega^e} \frac{\partial N_i}{\partial z} k \rho g \cos(\alpha) d\Omega \quad (\text{A9a})$$

$$\mathbf{F}_i^{\text{ext}} = - \sum_{e=1}^{n_{el}} \int_{\Omega^e} N_i E_v d\Omega. \quad (\text{A9b})$$

[58] Recalling from equations (3) and (4) that the conductance k and the capacitance C are both dependent on Φ , we note that the time-dependent matrix equation (A7) is nonlinear. Its linearized form is derived below. The Newton-Raphson method is then used to iteratively find the solution at each time step, and the backward-Euler scheme is used to step the solution forward in time.

[59] As a first step in the linearization process, we define the residual vector,

$$\mathbf{R}(\mathbf{d}) = \mathbf{M}(\mathbf{d}) \partial \mathbf{d} / \partial t + \mathbf{K}(\mathbf{d}) \mathbf{d} + \mathbf{F}^{\text{int}}(\mathbf{d}) - \mathbf{F}^{\text{ext}}. \quad (\text{A10})$$

It is obvious that $\mathbf{R} = 0$ if and only if (A7) is satisfied. For the purpose of linearization, we denote by $\mathbf{d}_{(n+1)}^{(p+1)}$ the unknown solution being sought in iteration $p + 1$ of time step $n + 1$, and by $\mathbf{d}_{(n+1)}^{(p)}$ the known solution obtained at the end of the preceding iteration of the same time step, and we write

$$\mathbf{d}_{(n+1)}^{(p+1)} = \mathbf{d}_{(n+1)}^{(p)} + \Delta \mathbf{d}_{(n+1)}^{(p+1)}. \quad (\text{A11})$$

Accordingly, a truncated Taylor-series expansion of $\mathbf{R}(\mathbf{d}_{(n+1)}^{(p+1)})$ gives

$$\mathbf{R}(\mathbf{d}_{(n+1)}^{(p+1)}) \approx \mathbf{R}(\mathbf{d}_{(n+1)}^{(p)}) + \left(\frac{\partial \mathbf{R}(\mathbf{d}_{(n+1)}^{(p)})}{\partial \mathbf{d}_{(n+1)}^{(p)}} \right) \Delta \mathbf{d}_{(n+1)}^{(p+1)}. \quad (\text{A12})$$

The right side of (A12) is made to vanish by solving

$$\mathbf{T} \Delta \mathbf{d}_{(n+1)}^{(p+1)} = \mathbf{S}, \quad (\text{A13a})$$

where the vector \mathbf{S} and the tangent matrix \mathbf{T} are defined as

$$\mathbf{S} := -\mathbf{R}(\mathbf{d}_{(n+1)}^{(p)}) \quad (\text{A13b})$$

$$\mathbf{T} := \frac{\partial \mathbf{R}(\mathbf{d}_{(n+1)}^{(p)})}{\partial \mathbf{d}_{(n+1)}^{(p)}} \quad (\text{A13c})$$

and obtained via the usual assembly process [see *Hughes, 2000*] from the corresponding element arrays, \mathbf{s} and \mathbf{t} , respectively. These are given by

$$\begin{aligned} s_i = & - \sum_j \int_{\Omega^e} \left[N_i C_{(n+1)}^{(p)} N_j \right] \left(\frac{(d_j)_{(n+1)}^{(p)} - (d_j)_n}{\Delta t} \right) d\Omega \\ & - \sum_j \int_{\Omega^e} \left[\frac{\partial N_i}{\partial z} k_{(n+1)}^{(p)} \frac{\partial N_j}{\partial z} \right] (d_j)_{(n+1)}^{(p)} d\Omega \\ & - \int_{\Omega^e} \frac{\partial N_i}{\partial z} k_{(n+1)}^{(p)} \rho g \cos(\alpha) d\Omega - \int_{\Omega^e} N_i E_v d\Omega \end{aligned} \quad (\text{A14a})$$

$$\begin{aligned}
t_{ij} = & \frac{1}{\Delta t} \int_{\Omega^e} N_i C_{(n+1)}^{(p)} N_j d\Omega + \int_{\Omega^e} \frac{\partial N_i}{\partial z} k_{(n+1)}^{(p)} \frac{\partial N_j}{\partial z} d\Omega \\
& + \sum_q \int_{\Omega^e} \left[N_i \left(\frac{\partial C_{(n+1)}^{(p)}}{\partial (\mathbf{d}_q)_{(n+1)}^{(p)}} \right) N_j \right] \left(\frac{(\mathbf{d}_q)_{(n+1)}^{(p)} - (\mathbf{d}_q)_{(n)}^{(p)}}{\Delta t} \right) d\Omega \\
& + \sum_q \int_{\Omega^e} \left[\frac{\partial N_i}{\partial z} \left(\frac{\partial k_{(n+1)}^{(p)}}{\partial (\mathbf{d}_q)_{(n+1)}^{(p)}} \right) \frac{\partial N_j}{\partial z} \right] (\mathbf{d}_q)_{(n+1)}^{(p)} d\Omega \\
& + \int_{\Omega^e} \frac{\partial N_i}{\partial z} \left(\frac{\partial k_{(n+1)}^{(p)}}{\partial (\mathbf{d}_j)_{(n+1)}^{(p)}} \right) \rho g \cos(\alpha) d\Omega, \quad (A14b)
\end{aligned}$$

where for compactness, $C_{(n+1)}^{(p)}$ denotes $C(\mathbf{d}_{(n+1)}^{(p)})$ and $k_{(n+1)}^{(p)}$ denotes $k(\mathbf{d}_{(n+1)}^{(p)})$.

[60] **Acknowledgments.** The authors thank Michiaki Sugita and three anonymous referees for their helpful comments. We acknowledge the comments and assistance we received from Yao Li Chuang. We also thank Tea Yeon Kim, Eui Joong Kim, Ilina Stanciulescu, and Huidi Ji for assistance in the model development, Mathieu Therezien and Kristen Goris for additional simulations, and Robert Walko, Amilcare Porporato, Edoardo Daly, Kivanc Ekici, Gary Ybarra, Stacy Tatum, and Zbigniew Kabala for assistance and advice. This research was supported by the Office of Science (BER), U.S. Department of Energy, through the Terrestrial Carbon Processes Program (TCP), grant DE-FG02-00ER63015 and grant DE-FG02-95ER62083; by the BER's Southeast Regional Center (SERC) of the National Institute for Global Environmental Change (NIGEC) under Cooperative Agreement DEFC02-03ER63613; by the National Oceanic and Atmospheric Administration (NOAA), grant NA96GP0479; and by the National Science Foundation (NSF), grant DEB-0453296. The views expressed herein are those of the authors and do not necessarily reflect the views of these agencies.

References

- Addington, R. N., R. J. Mitchell, R. Oren, and L. A. Donovan (2004), Stomatal sensitivity to vapor pressure deficit and its relationship to hydraulic conductance in *Pinus palustris*, *Tree Physiol.*, *24*, 561–569.
- Alder, N. N., W. T. Pockman, J. S. Sperry, and S. Nuismer (1997), Use of centrifugal force in the study of xylem cavitation, *J. Exp. Bot.*, *48*, 665–674.
- Arbogast, T., M. Obeyesekere, and M. F. Wheeler (1993), Numerical-methods for the simulation of flow in root-soil systems, *SIAM J. Numer. Anal.*, *30*, 1677–1702.
- Aumann, C. A., and E. D. Ford (2002a), Modeling tree water flow as an unsaturated flow through a porous medium, *J. Theor. Biol.*, *219*, 415–429.
- Aumann, C. A., and E. D. Ford (2002b), Parameterizing a model of Douglas fir water flow using a tracheid-level model, *J. Theor. Biol.*, *219*, 431–462.
- Baldocchi, D. (1992), A Lagrangian random-walk model for simulating water-vapor, CO₂ and sensible heat-flux densities and scalar profiles over and within a soybean canopy, *Boundary Layer Meteorol.*, *61*, 113–144.
- Baldocchi, D., and T. Meyers (1998), On using eco-physiological, micro-meteorological and biogeochemical theory to evaluate carbon dioxide, water vapor and trace gas fluxes over vegetation: A perspective, *Agric. For. Meteorol.*, *90*, 1–25.
- Borchert, R. (1994), Soil and stem water storage determine phenology and distribution of tropical dry forest trees, *Ecology*, *75*, 1437–1449.
- Brodribb, T. J., and N. M. Holbrook (2004), Diurnal depression of leaf hydraulic conductance in a tropical tree species, *Plant Cell Environ.*, *27*, 820–827.
- Campbell, G. S., and J. M. Norman (1998), *An Introduction to Environmental Biophysics*, 2nd ed., 286 pp., Springer, New York.
- Chuang, Y., R. Oren, A. L. Bertozzi, N. Phillips, and G. Katul (2005), The porous media model for the hydraulic system of a tree: From sap flux data to transpiration rate, *Ecol. Modell.*, in press.
- Collatz, G. J., J. T. Ball, C. Grivet, and J. A. Berry (1991), Physiological and environmental regulation of stomatal conductance, photosynthesis and transpiration: A model that includes a laminar boundary layer, *Agric. For. Meteorol.*, *54*, 107–136.
- Cruziat, P., H. Cochard, and T. Améglio (2002), Hydraulic architecture of trees: Main concepts and results, *Ann. For. Sci.*, *59*, 723–752.
- Domec, J. C., and B. L. Gartner (2003), Relationship between growth rates and xylem hydraulic characteristics in young, mature and old-growth ponderosa pine trees, *Plant Cell Environ.*, *26*, 471–483.
- Ewers, B. E., R. Oren, N. Phillips, M. Strömgren, and S. Linder (2001), Mean canopy stomatal conductance responses to water and nutrient availabilities in *Picea abies* and *Pinus taeda*, *Tree Physiol.*, *21*, 841–850.
- Farquhar, G. D., S. V. Caemmerer, and J. A. Berry (1980), A biochemical model of photosynthetic CO₂ assimilation in leaves of C-3 species, *Planta*, *149*, 78–90.
- Feild, T. S., T. Brodribb, and M. Holbrook (2002), Hardly a relict: Freezing and the evolution of vesselless wood in Winteraceae, *Evolution*, *56*, 464–478.
- Früh, T., and W. Kurth (1999), The hydraulic system of trees: Theoretical framework and numerical simulation, *J. Theor. Biol.*, *201*, 251–270.
- Goldstein, G., J. L. Andrade, F. C. Meinzer, N. M. Holbrook, J. Cavelier, P. Jackson, and A. Celis (1998), Stem water storage and diurnal patterns of water use in tropical forest canopy trees, *Plant Cell Environ.*, *21*, 397–406.
- Hacke, U. G., J. S. Sperry, B. E. Ewers, D. S. Ellsworth, K. V. R. Schäfer, and R. Oren (2000), Influence of soil porosity on water use in *Pinus taeda*, *Oecologia*, *124*, 495–505.
- Herzog, K. M., R. Thum, G. Kronfuss, H. J. Heldstab, and R. Häslar (1998), Patterns and mechanisms of transpiration in a large sub alpine Norway spruce (*Picea abies* (L.) Karst.), *Ecol. Res.*, *13*, 105–116.
- Hubbard, R. M., M. G. Ryan, V. Stiller, and J. S. Sperry (2001), Stomatal conductance and photosynthesis vary linearly with plant hydraulic conductance in ponderosa pine, *Plant Cell Environ.*, *24*, 113–121.
- Hughes, T. J. R. (2000), *The Finite Element Method: Linear Static and Dynamic Finite Element Analysis*, 682 pp., Dover, Mineola, N. Y.
- Jones, H. G. (1992), Plant water relations, in *Plants and Microclimate: A Quantitative Approach to Environmental Plant Physiology*, edited by G. J. Hamlyn, pp. 72–105, Cambridge Univ. Press, New York.
- Katul, G., R. Leuning, and R. Oren (2003), Relationship between plant hydraulic and biochemical properties derived from a steady-state coupled water and carbon transport model, *Plant Cell Environ.*, *26*, 339–350.
- Köstner, B. (2001), Evaporation and transpiration from forests in central Europe: Relevance of patch-level studies for spatial scaling, *Meteorol. Atmos. Phys.*, *76*, 69–82.
- Kumagai, T. (2001), Modeling water transportation and storage in sapwood: Model development and validation, *Agric. For. Meteorol.*, *109*, 105–115.
- Lai, C. T., G. Katul, D. Ellsworth, and R. Oren (2000a), Modeling vegetation-atmosphere CO₂ exchange by a coupled Eulerian-Lagrangian approach, *Boundary Layer Meteorol.*, *95*, 91–122.
- Lai, C. T., G. Katul, R. Oren, D. Ellsworth, and K. Schäfer (2000b), Modeling CO₂ and water vapor turbulent flux distributions within a forest canopy, *J. Geophys. Res.*, *105*, 26,333–26,351.
- Lai, C. T., G. Katul, J. Butnor, D. Ellsworth, and R. Oren (2002), Modeling nighttime ecosystem respiration by a constrained source optimization method, *Global Change Biol.*, *8*, 124–141.
- Lefsky, M. A., W. B. Cohen, G. G. Parker, and D. J. Harding (2002), Lidar remote sensing for ecosystem studies, *Bioscience*, *52*, 19–30.
- Leonardo da Vinci (1970), Botany for painters and elements of landscape painting, in *The Notebooks of Leonardo da Vinci Compiled and Edited From the Original Manuscripts*, vol. 1, edited by J. P. Richter, pp. 203–240, Dover, Mineola, N. Y.
- Leuning, R. (1995), A critical-appraisal of a combined stomatal-photosynthesis model for C-3 plants, *Plant Cell Environ.*, *18*, 339–355.
- Leuning, R. (1997), Scaling to a common temperature improves the correlation between the photosynthesis parameters J (max) and V-cmax, *J. Exp. Bot.*, *48*, 345–347.
- Leuning, R. (2002), Temperature dependence of two parameters in a photosynthesis model, *Plant Cell Environ.*, *25*, 1205–1210.
- Leuning, R., F. M. Kelliher, D. G. G. Depury, and E. D. Schulze (1995), Leaf nitrogen, photosynthesis, conductance and transpiration: Scaling from leaves to canopies, *Plant Cell Environ.*, *18*, 1183–1200.
- Liang, X., D. P. Lettenmaier, E. F. Wood, and S. J. Burges (1994), A simple hydrologically based model of land-surface water and energy fluxes for general circulation models, *J. Geophys. Res.*, *99*, 14,415–14,428.
- Lindenmayer, A. (1968), Mathematical models for cellular interaction in development, *J. Theor. Biol.*, *18*, 280–315.
- Lindenmayer, A. (1971), Development systems without cellular interaction, their languages and grammars, *J. Theor. Biol.*, *30*, 455–484.

- Maherali, H., and E. H. DeLucia (2001), Influence of climate-driven shifts in biomass allocation on water transport and storage in ponderosa pine, *Oecologia*, *129*, 481–491.
- Mayr, S., F. Schwiendbacher, and H. Bauer (2003), Winter at the alpine timberline: Why does embolism occur in Norway spruce but not in stone pine?, *Plant Physiol.*, *131*, 780–792.
- McCulloh, K. A., J. S. Sperry, and F. R. Adler (2003), Water transport in plants obeys Murray's law, *Nature*, *421*, 939–942.
- Meinzer, F. C., S. A. James, G. Goldstein, and D. Woodruff (2003), Whole-tree water transport scales with sapwood capacitance in tropical forest canopy trees, *Plant Cell Environ.*, *26*, 1147–1155.
- Murray, C. D. (1926), The physiological principle of minimum work: I. The vascular system and the cost of blood volume, *Proc. Natl. Acad. Sci. U. S. A.*, *12*, 207–214.
- Nishida, K., R. R. Nemani, S. W. Running, and J. M. Glassy (2003), An operational remote sensing algorithm of land surface evaporation, *J. Geophys. Res.*, *108*(D9), 4270, doi:10.1029/2002JD002062.
- Oren, R., K. S. Werk, and E. D. Schulze (1986), Relationships between foliage and conducting xylem in *Picea abies* (L.) Karst, *Trees Struct. Funct.*, *1*, 61–69.
- Oren, R., R. Zimmermann, and J. Terborgh (1996), Transpiration in upper Amazonia floodplain and upland forests in response to drought-breaking rains, *Ecology*, *77*, 968–973.
- Oren, R., N. Phillips, G. Katul, B. E. Ewers, and D. E. Pataki (1998), Scaling xylem sap flux and soil water balance and calculating variance: A method for partitioning water flux in forests, *Ann. For. Sci.*, *55*, 191–216.
- Oren, R., N. Phillips, B. E. Ewers, D. E. Pataki, and J. P. Mezonigal (1999a), Sap-flux-scaled transpiration responses to light, vapor pressure deficit, and leaf area reduction in a flooded *Taxodium distichum* forest, *Tree Physiol.*, *19*, 337–347.
- Oren, R., J. S. Sperry, G. G. Katul, D. E. Pataki, B. E. Ewers, N. Phillips, and K. V. R. Schäfer (1999b), Survey and synthesis of intra- and interspecific variation in stomatal sensitivity to vapor pressure deficit, *Plant Cell Environ.*, *22*, 1515–1526.
- Oren, R., J. S. Sperry, B. E. Ewers, D. E. Pataki, N. Phillips, and J. P. Mezonigal (2001), Sensitivity of mean canopy stomatal conductance to vapor pressure deficit in a flooded *Taxodium distichum* L. forest: Hydraulic and non-hydraulic effects, *Oecologia*, *126*, 21–29.
- Pataki, D. E., R. Oren, and W. K. Smith (2000), Sap flux of co-occurring species in a western subalpine forest during seasonal soil drought, *Ecology*, *81*, 2557–2566.
- Phillips, N., R. Oren, and R. Zimmermann (1996), Radial patterns of xylem sap flow in non-, diffuse- and ring-porous tree species, *Plant Cell Environ.*, *19*, 983–990.
- Phillips, N., A. Nagchadhuri, R. Oren, and G. Katul (1997), Time constant for water transport in loblolly pine trees estimated from time series of evaporative demand and stem sap-flow, *Trees Struct. Funct.*, *11*, 412–419.
- Phillips, N., R. Oren, R. Zimmermann, and S. J. Wright (1999), Temporal patterns of water flux in trees and lianas in a Panamanian moist forest, *Trees Struct. Funct.*, *14*, 116–123.
- Phillips, N., J. Bergh, R. Oren, and S. Linder (2001), Effects of nutrition and soil water availability on water use in a Norway spruce stand, *Tree Physiol.*, *21*, 851–860.
- Phillips, N. G., R. Oren, J. Licata, and S. Linder (2004), Time series diagnosis of tree hydraulic characteristics, *Tree Physiol.*, *24*, 879–890.
- Pielke, R. A., et al. (1992), A comprehensive meteorological modeling system—RAMS, *Meteorol. Atmos. Phys.*, *49*, 69–91.
- Poggi, D., A. Porporato, L. Ridolfi, J. D. Albertson, and G. G. Katul (2004), The effect of vegetation density on canopy sub-layer turbulence, *Boundary Layer Meteorol.*, *111*, 565–587.
- Prusinkiewicz, P., and A. Lindenmayer (1990), *The Algorithmic Beauty of Plants (The Virtual Laboratory)*, 228 pp., Springer, New York.
- Prusinkiewicz, P., M. Hammel, J. Hanan, and R. Mech (1997), Visual models of plant development, in *Handbook of Formal Languages*, vol. 3, edited by G. Rozenberg and A. Salomaa, pp. 535–597, Springer, New York.
- Rayment, M. B., D. Loustau, and P. G. Jarvis (2000), Measuring and modeling conductances of black spruce at three organizational scales: Shoot, branch and canopy, *Tree Physiol.*, *20*, 713–723.
- Ryan, M. G., B. J. Bond, B. E. Law, R. M. Hubbard, D. Woodruff, E. Cienciala, and J. Kucera (2000), Transpiration and whole-tree conductance in ponderosa pine trees of different heights, *Oecologia*, *124*, 553–560.
- Schäfer, K. V. R., R. Oren, and J. D. Tenhunen (2000), The effect of tree height on crown level stomatal conductance, *Plant Cell Environ.*, *23*, 365–375.
- Schäfer, K. V. R., R. Oren, C. T. Lai, and G. G. Katul (2002), Hydrologic balance in an intact temperate forest ecosystem under ambient and elevated atmospheric CO₂ concentration, *Global Change Biol.*, *8*, 895–911.
- Schäfer, K. V. R., R. Oren, D. S. Ellsworth, C. T. Lai, J. D. Herrick, A. C. Finzi, D. D. Richter, and G. G. Katul (2003), Exposure to an enriched CO₂ atmosphere alters carbon assimilation and allocation in a pine forest ecosystem, *Global Change Biol.*, *9*, 1378–1400.
- Schulte, P. J., and J. R. Brooks (2003), Branch junctions and the flow of water through xylem in Douglas-fir and ponderosa pine stems, *J. Exp. Bot.*, *54*, 1597–1605.
- Schulte, P. J., and D. G. Costa (1996), A mathematical description of water flow through plant tissues, *J. Theor. Biol.*, *180*, 61–70.
- Sellers, P. J., S. O. Los, C. J. Tucker, C. O. Justice, D. A. Dazlich, G. J. Collatz, and D. A. Randall (1996a), A revised land surface parameterization (SiB2) for atmospheric GCMs: 2. The generation of global fields of terrestrial biophysical parameters from satellite data, *J. Clim.*, *9*, 706–737.
- Sellers, P. J., D. A. Randall, G. J. Collatz, J. A. Berry, C. B. Field, D. A. Dazlich, C. Zhang, G. D. Collelo, and L. Bounoua (1996b), A revised land surface parameterization (SiB2) for atmospheric GCMs: 1. Model formulation, *J. Clim.*, *9*, 676–705.
- Siau, J. F. (1983), A proposed theory for non-isothermal unsteady state transport of moisture in wood, *Wood Sci. Technol.*, *17*, 75–77.
- Sperry, J. S. (1986), Relationship of xylem embolism to xylem pressure potential, stomatal closure, and shoot morphology in the palm *Rhapis excelsa*, *Plant Physiol.*, *80*, 110–116.
- Sperry, J. S. (2000), Hydraulic constraints on plant gas exchange, *Agric. For. Meteorol.*, *104*, 13–23.
- Sperry, J. S., J. R. Donnelly, and M. T. Tyree (1988), A method for measuring hydraulic conductivity and embolism in xylem, *Plant Cell Environ.*, *11*, 35–40.
- Sperry, J. S., K. L. Nichols, J. E. M. Sullivan, and S. E. Eastlack (1994), Xylem embolism in ring-porous, diffuse-porous, and coniferous trees of northern Utah and interior Alaska, *Ecology*, *75*, 1736–1752.
- Sperry, J. S., F. R. Adler, G. S. Campbell, and J. P. Comstock (1998), Limitation of plant water use by rhizosphere and xylem conductance: Results from a model, *Plant Cell Environ.*, *21*, 347–359.
- Sperry, J. S., U. G. Hacke, R. Oren, and J. P. Comstock (2002), Water deficits and hydraulic limits to leaf water supply, *Plant Cell Environ.*, *25*, 251–263.
- Sperry, J. S., V. Stiller, and U. G. Hacke (2003), Xylem hydraulics and the soil-plant-atmosphere continuum: Opportunities and unresolved issues, *Agron. J.*, *95*, 1362–1370.
- Stenberg, P. (1995), Penumbra in within-shoot and between-shoot shading in conifers and its significance for photosynthesis, *Ecol. Modell.*, *77*, 215–231.
- Szilard, A. L., and R. E. Quinton (1979), An interpretation for DOL systems by computer graphics, *Sci. Terrapin*, *4*, 8–13.
- Tanaka, S., and T. Sugimura (2001), A new frontier of remote sensing from IKONOS images, *Int. J. Remote Sens.*, *22*, 1–5.
- Tyree, M. T. (2003), The ascent of water, *Nature*, *423*, 923.
- Tyree, M. T., and F. W. Ewers (1991), The hydraulic architecture of trees and other woody-plants, *New Phytol.*, *119*, 345–360.
- Tyree, M. T., and J. S. Sperry (1989), Vulnerability of xylem to cavitation and embolism, *Annu. Rev. Plant Physiol. Plant Mol. Biol.*, *40*, 19–38.
- Walko, R. L., et al. (2000), Coupled atmosphere-biophysics-hydrology models for environmental modeling, *J. Appl. Meteorol.*, *39*, 931–944.
- Wood, E. F., D. P. Lettenmaier, and V. G. Zartarian (1992), A land-surface hydrology parameterization with subgrid variability for general-circulation models, *J. Geophys. Res.*, *97*, 2717–2728.
- Zweifel, R., H. Item, and R. Häsler (2001), Link between diurnal stem radius changes and tree water relations, *Tree Physiol.*, *21*, 869–877.
- Zweifel, R., J. P. Bohm, and R. Häsler (2002), Midday stomatal closure in Norway spruce: Reactions in the upper and lower crown, *Tree Physiol.*, *22*, 1125–1136.

R. Avissar, G. Bohrer, D. Drewry, T. A. Laursen, and H. Mourad, Department of Civil and Environmental Engineering, Box 90287, Duke University, Durham, NC 27708-0287, USA. (gb16@duke.edu)
G. G. Katul, R. Oren, and D. Poggi, Nicholas School of the Environment and Earth Sciences, Box 90328, Duke University, Durham, NC 27708, USA.